LETTER

doi:10.1038/nature13159

Sensory stimulation shifts visual cortex from synchronous to asynchronous states

Andrew Y. Y. Tan[1,2]*, Yuzhi Chen[1,2,3]*, Benjamin Scholl[1,2]*, Eyal Seidemann[1,2,3] & Nicholas J. Priebe[1,2]

In the mammalian cerebral cortex, neural responses are highly variable during spontaneous activity and sensory stimulation. To explain this variability, the cortex of alert animals has been proposed to be in an asynchronous high-conductance state in which irregular spiking arises from the convergence of large numbers of uncorrelated excitatory and inhibitory inputs onto individual neurons[1–4]. Signatures of this state are that a neuron's membrane potential (V_m) hovers just below spike threshold, and its aggregate synaptic input is nearly Gaussian, arising from many uncorrelated inputs[1–4]. Alternatively, irregular spiking could arise from infrequent correlated input events that elicit large fluctuations in V_m (refs 5, 6). To distinguish between these hypotheses, we developed a technique to perform whole-cell V_m measurements from the cortex of behaving monkeys, focusing on primary visual cortex (V1) of monkeys performing a visual fixation task. Here we show that, contrary to the predictions of an asynchronous state, mean V_m during fixation was far from threshold (14 mV) and spiking was triggered by occasional large spontaneous fluctuations. Distributions of V_m values were skewed beyond that expected for a range of Gaussian input[6,7], but were consistent with synaptic input arising from infrequent correlated events[5,6]. Furthermore, spontaneous fluctuations in V_m were correlated with the surrounding network activity, as reflected in simultaneously recorded nearby local field potential. Visual stimulation, however, led to responses more consistent with an asynchronous state: mean V_m approached threshold, fluctuations became more Gaussian, and correlations between single neurons and the surrounding network were disrupted. These observations show that sensory drive can shift a common cortical circuitry from a synchronous to an asynchronous state.

Cortical neurons show variable activity even after efforts are taken to fix temporal variations in sensory stimuli and attentional state[8]. This ongoing activity affects stimulus encoding and synaptic plasticity[9], but its neural basis is not well understood. One hypothesis is that the variable activity in alert animals arises from connections between numerous uncorrelated excitatory and inhibitory inputs[1–4]. Such a network is consistent with studies of neural architecture[10], and shows spiking statistics similar to those measured in extracellular studies[8]. Predictions of this hypothesis[2–4,6,7] are that numerous uncorrelated inputs (Fig. 1a, bottom) cause V_m to hover near spike threshold (Fig. 1a, top left) and to show distributions that are near Gaussian or skewed with tails at hyperpolarized potentials (Fig. 1a, top right). In contrast, neurons may receive correlated input[5,6] (Fig. 1b, bottom) such that V_m lies far below threshold and shows infrequent large excursions (Fig. 1b, top left), forming skewed distributions with tails at depolarized potentials (Fig. 1b, top right). Measurements of V_m from awake, non-behaving cats suggest an asynchronous state[11], but are also consistent with correlated input[12]. Data from behaving rodents in various attentional states have suggested different pictures[13–16], but equivocally, because of the potential contributions of uncontrolled sensory inputs and attentional states to V_m dynamics. Extracellular recordings in drowsy humans have demonstrated correlated spontaneous cortical activity, leaving open the possibility that correlations are absent during alertness[17]. Accordingly, we performed the first whole-cell V_m measurements from the cortex of monkeys actively engaged in a visual fixation task, allowing us to examine V_m in single V1 neurons of alert primates while minimizing variability due to sensory stimuli, eye movements and attentional state.

We obtained intracellular[18], whole-cell[19,20], current-clamp measurements of V_m from 31 V1 neurons in three macaque monkeys while they viewed gratings of different orientations (see Supplementary Information and Supplementary Video). Each trial began when a fixation spot was displayed at the centre of a monitor in front of the monkey. The monkey had to shift gaze to the fixation point and maintain tight fixation for at least 1,500 ms to receive a reward. A drifting sinusoidal grating was presented for 1,000 ms while the monkey was maintaining strict fixation. We analysed V_m during the fixation period only from trials in which the monkey performed the task successfully. V1 neurons were orientation-selective, and were classified as simple or complex (Supplementary Information and Extended Data Fig. 1).

Comparison of V_m in blank trials in which no visual stimulus was presented (Fig. 2a–c, left) with suprathreshold responses evoked by preferred orientation gratings (Fig. 2a–c, right) shows that blank trial V_m was generally far from spike threshold. There were occasional large depolarizations during blank trials, which were manifested in the positive skewness of V_m amplitude histograms: these had longer tails at depolarized potentials, even though traces had had spikes removed (Fig. 2a–c, left, orange histograms; see also Supplementary Information and Extended Data Fig. 2). Across neurons, the median distance between blank trial

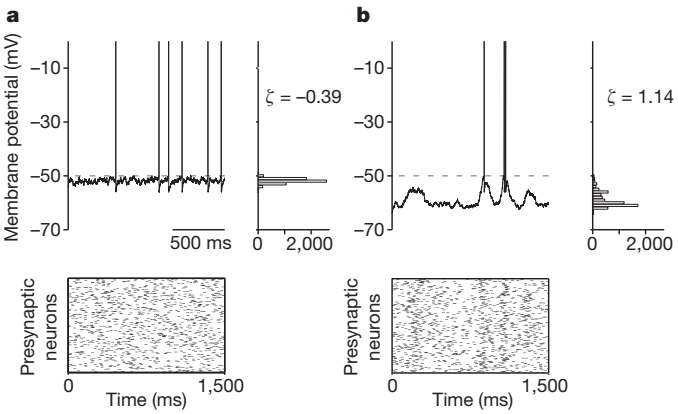

Figure 1 | V_m characteristics depend on network state. **a**, Diagram of an asynchronous high-conductance state. A neuron receives numerous uncorrelated inputs (bottom), V_m hovers near spike threshold (top left), forming distributions with low or negative skewness ζ (top right). **b**, A neuron may instead receive correlated inputs (bottom) such that V_m lies farther from spike threshold and shows occasional large fluctuations (top left), forming distributions with high skewness ζ (top right).

[1]Center for Perceptual Systems, University of Texas, Austin, Texas 78712, USA. [2]Department of Neuroscience, College of Natural Sciences, University of Texas, Austin, Texas 78712, USA. [3]Department of Psychology, University of Texas, Austin, Texas 78712, USA.
*These authors contributed equally to this work.

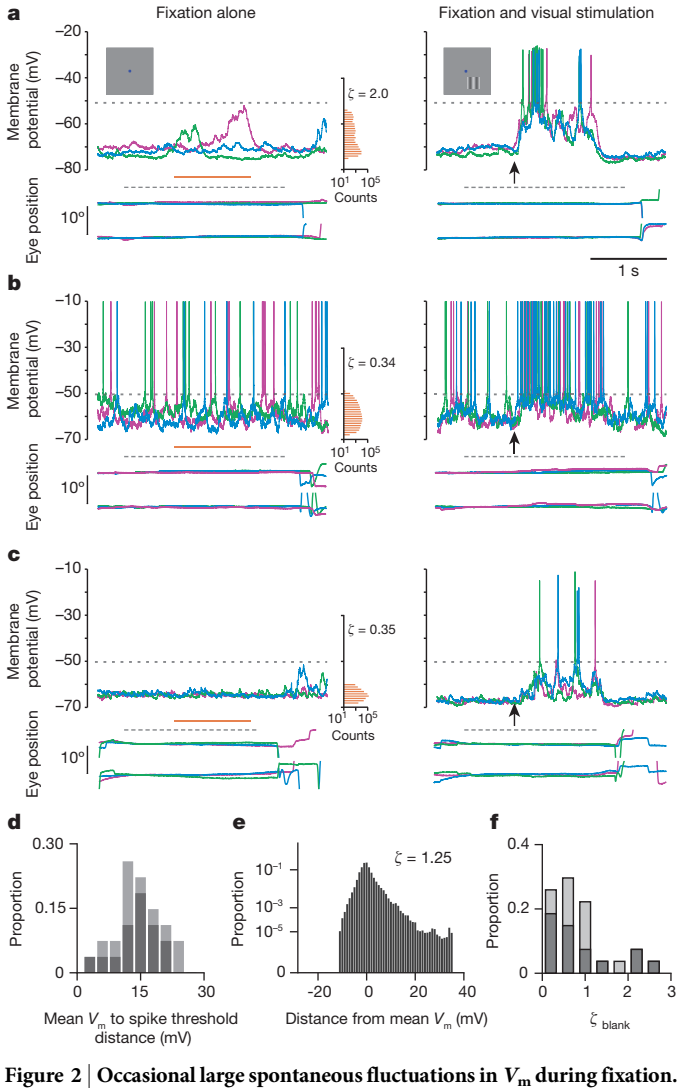

Figure 2 | Occasional large spontaneous fluctuations in V_m during fixation. **a–c**, V_m (top), horizontal and vertical eye position (bottom) from three blank trials, and corresponding histograms from the period indicated by the orange line (left). Horizontal scales for the histograms are logarithmic. Right: traces from three preferred orientation trials; the arrow indicates stimulus onset. Lower and upper dashed lines indicate the period of required fixation and the spike threshold, respectively. Results in **a**, **b** and **c** are from different neurons. **d**, Distribution across neurons of distance between mean V_m during blank trials and spike threshold ($n = 26$). **e**, The population distribution of V_m for blank trials is the average of each neuron's normalized mean-subtracted distribution. **f**, Distribution across neurons of blank trial V_m skewness. Light and dark bars in **d** and **f** indicate simple and complex cells, respectively.

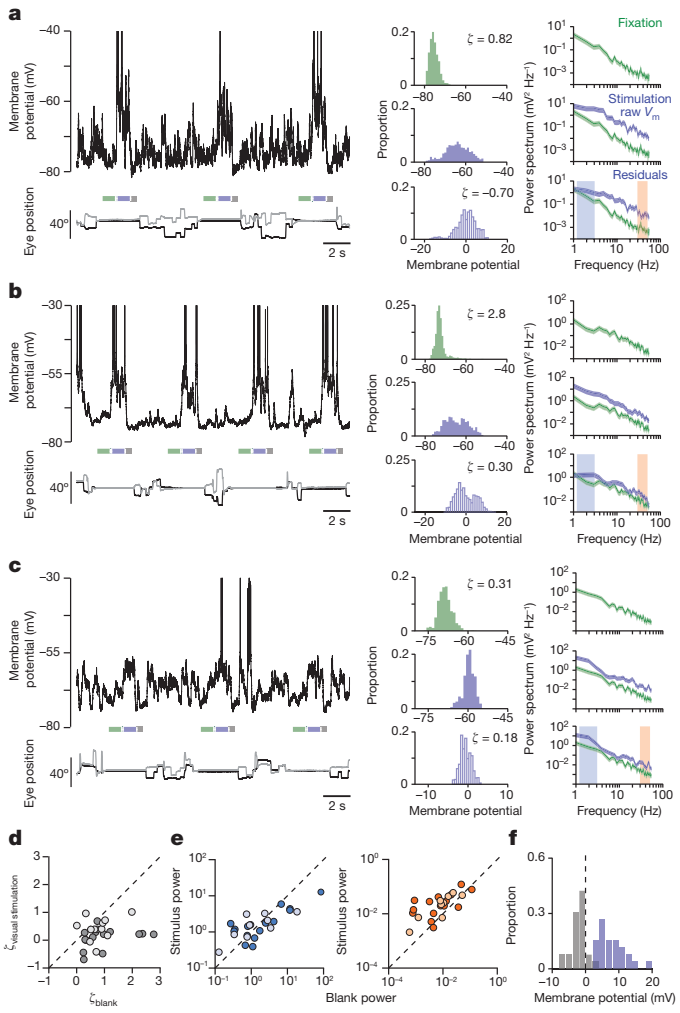

Figure 3 | Visually evoked V_m is closer to threshold and has more Gaussian fluctuations. **a–c**, Left: V_m (top) and eye position (bottom) over pre-stimulus, stimulus and post-stimulus periods during fixation (green, lavender and grey bars, respectively) and inter-trial periods. Right: pre-stimulus, stimulus period raw value and residual (green, lavender-filled and lavender-outlined respectively) histograms and power spectra; shaded areas indicate low and high frequency ranges. Results in **a**, **b** and **c** are from different neurons. **d**, Skewness of V_m residuals during the preferred orientation versus that during blank trials, for each neuron. **e**, Mean power in V_m residuals during blank versus visual stimulation at low frequencies (0.5–4 Hz, left) and high frequencies (30–50 Hz, right). **f**, Distribution across neurons of mean V_m during stimulus (lavender) and post-stimulus (grey) periods, relative to mean pre-stimulus V_m. Light and dark circles in **d** and **e** indicate simple and complex cells, respectively.

V_m and spike threshold was 13.9 mV (Fig. 2d). The median skewness of 0.72 (Fig. 2e, f) differs from the near zero or negative skewness expected for a range of Gaussian input (Fig. 1a; see also Supplementary Information and Extended Data Fig. 2c), but is consistent with synaptic input arising from infrequent correlated events (Fig. 1b). These data show that in the absence of visual stimulation, V1 of macaques performing a visual fixation task is not in an asynchronous high-conductance state[1–4].

By comparison, visual stimulation depolarized neurons (Fig. 2a–c, right, and Fig. 3a–c) and decreased the skewness of V_m deviations from the mean (Fig. 3a–c; see also Supplementary Information and Extended Data Fig. 3), an effect that was significant across the population (Fig. 3d; Wilcoxon signed-rank test, $P < 0.0001$; see also Supplementary Information and Extended Data Fig. 4). Together with observed increases in membrane conductance during visual stimulation[21,22] (Supplementary Information and Extended Data Fig. 5), these results suggest that visual stimulation shifts the cortical network towards an asynchronous high-conductance state[1–4].

Visual stimulation also caused significant changes in the power of V_m fluctuations. Membrane potential showed greater power at low frequencies than at high frequencies during fixation, both before and during visual stimulation. Visual stimulation increased the power of V_m fluctuations from the trial average (that is, residuals) at high frequencies (30–50 Hz) but did not cause systematic changes at low frequencies (0.5–4 Hz) (Fig. 3a–c, e; Wilcoxon signed-rank test, $P = 0.76$ (0.5–4 Hz), $P = 0.001$ (30–50 Hz); see also Supplementary Information and Extended Data Fig. 6). Post-stimulus V_m was typically below pre-stimulus values (Fig. 3f; Wilcoxon signed-rank test $P < 0.0001$).

If, as our intracellular recordings suggest, visual stimulation shifts V1 towards an asynchronous state, there should be a concomitant reduction in the correlation between V_m and the surrounding network, as reflected in the simultaneously recorded nearby local field potential (LFP).

This was the case. During fixation with no visual stimulus, deflections indicating spontaneous increases in activity are evident in V_m and LFP (Fig. 4a, left, depolarization for V_m, downward deflections for LFP). These deflections are coincident in both signals (asterisks in Fig. 4a); across our population, the zero-lag V_m–LFP cross-correlation was negative during blank trials, reflecting coincident activation of the network and individual neurons (Fig. 4d, green, median cross-correlation −0.24; Wilcoxon signed-rank test, $P < 0.01$). To determine whether visual stimulation alters this relationship we examined V_m–LFP correlations after trial averages had been subtracted (Fig. 4b, c, centre panels). Correlations declined when drifting gratings were presented (Fig. 4b–d; Wilcoxon signed-rank test, $P < 0.01$), such that the median cross-correlation was nearer zero (Fig. 4d, lavender; Wilcoxon signed-rank test, $P = 0.91$), providing further evidence that visual stimulation drives V1 towards an asynchronous state. The visually-evoked decline in V_m-LFP correlation was apparent for low frequency (0.5–4 Hz), but not high frequency fluctuations (Fig. 4e; Wilcoxon signed-rank test, $P < 0.01$ (0.5–4 Hz), $P = 0.13$ (30–50 Hz)); V_m-LFP coherence decreased at low (0.5–4 Hz), but not high frequencies (30–50 Hz) (Fig. 4b, c, right, and Fig. 4f; Wilcoxon signed-rank test, $P < 0.05$ (0.5–4 Hz), $P = 0.34$ (30–50 Hz); see also Supplementary Information and Extended Data Fig. 7).

We have shown that in the absence of visual stimulation, V1 in alert behaving primates is not in an asynchronous high-conductance state[1–4]. Rather, spontaneous V_m fluctuations are non-Gaussian and characterized by occasional excursions from rest, consistent with synaptic input arising from infrequent correlated events[5,6]. In our recordings, sensory stimulation drove V1 towards an asynchronous state, as visually evoked V_m was closer to spike threshold, showed more Gaussian fluctuations and became less correlated with low-frequency LFP. The visually evoked reduction in correlation between V_m and LFP is consistent with previously reported decreases in spiking correlations[23,24]. In an analogous fashion, the correlated activity patterns observed in mouse sensory cortex[14] during quiet wakefulness are disrupted by thalamic activation[25]. (See also Supplementary Information and Extended Data Fig. 8.) Our records focused on activity in superficial cortical layers; membrane potential characteristics may differ across layers, potentially reflecting laminar specificity in network state[26].

How can cortical circuitry support synchronous and asynchronous states? One salient difference between the states was the amount of external input: without visual stimulation the thalamic drive to cortex is weak, whereas visual stimulation activates those afferents. We propose that this difference in afferent drive explains the shift in network state. Our proposal unifies observation and theory: a lower input spike rate reduces synaptic input so that V_m lies further from threshold; postsynaptic potentials due to different sources are less likely to overlap in time and instead appear as distinct events. Crucially, theory indicates that a low thalamic

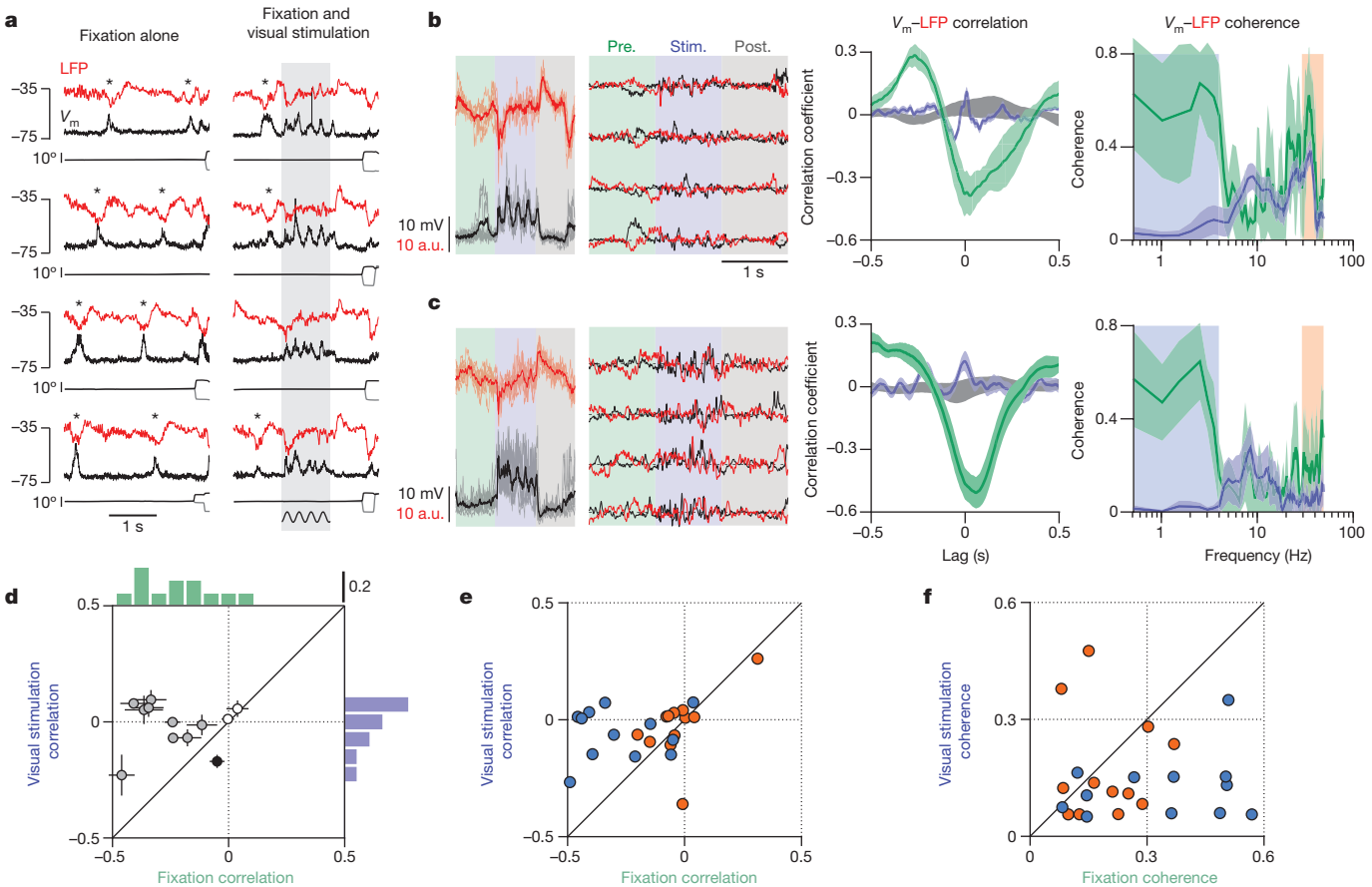

Figure 4 | Magnitude of V_m–LFP cross-correlation decreases during visual stimulation. **a**, Four trials of V_m (black) with simultaneously recorded LFP (red) and eye position (thin black traces) during the blank (left) and the preferred orientation (right) from one neuron. **b**, **c**, Left: V_m and LFP from four trials with superimposed trial average. Centre: traces with trial averages subtracted. Pre., pre-stimulation; stim., stimulation; post., post-stimulation. Right: V_m–LFP cross-correlation functions and coherence magnitudes for blank (green) and stimulus (lavender) periods, and shuffled stimulus trials (grey). Shaded areas show bootstrapped s.e.m. for cross-correlation functions, and jack-knifed 95% confidence intervals for coherence magnitudes. Results in **b** and **c** are from different neurons. **d**, Zero-lag V_m–LFP cross-correlation during visual stimulation (lavender) versus blank trials (green) for each neuron, and corresponding marginal histograms. Medium and dark filled circles indicate cross-correlations that were respectively greater or less during visual stimulation than blank trials (Wilcoxon signed-rank test, $P < 0.05$). **e**, Zero-lag V_m–LFP cross-correlation at low frequencies (0.5–4 Hz, blue) and high frequencies (30–50 Hz, orange). **f**, Root-mean-square V_m–LFP coherence magnitudes at low frequencies (0.5–4 Hz, blue) and high frequencies (30–50 Hz, orange).

spike rate destabilizes the asynchronous state towards low-frequency correlations[4,27,28], but higher thalamic spike rates drive the network towards an asynchronous state in which correlations weaken[4,27,28], as observed in our data. It is clear that external drive alters the cortical state[25], but internal factors are also essential. In extrastriate cortex, attention causes an increase in overall response that is also accompanied by a decline in the correlation between neurons[29,30]. Explaining how these external and internal drives are synthesized will require understanding how V1 interacts with downstream areas.

METHODS SUMMARY

Macaque monkeys were trained to perform a visual fixation task (see also Supplementary Information and Extended Data Fig. 9), and implanted with recording chambers. Blind *in vivo* whole-cell recordings were performed[19,20]. Patch pipettes were filled with (in mM) 135 potassium gluconate, 4 NaCl, 0.5 EGTA, 2 $MgATP^{2-}$, 10 phosphocreatine disodium, 10 HEPES, pH adjusted to 7.3 with KOH (Sigma-Aldrich) (see also Supplementary Information and Extended Data Fig. 10).

Online Content Any additional Methods, Extended Data display items and Source Data are available in the online version of the paper; references unique to these sections appear only in the online paper.

Received 27 September 2013; accepted 17 February 2014.
Published online 30 March 2014.

1. van Vreeswijk, C. & Sompolinsky, H. Chaos in neuronal networks with balanced excitatory and inhibitory activity. *Science* **274,** 1724–1726 (1996).
2. van Vreeswijk, C. & Sompolinsky, H. Chaotic balanced state in a model of cortical circuits. *Neural Comput.* **10,** 1321–1371 (1998).
3. Kumar, A., Schrader, S., Aertsen, A. & Rotter, S. The high-conductance state of cortical networks. *Neural Comput.* **20,** 1–43 (2008).
4. Renart, A. *et al.* The asynchronous state in cortical circuits. *Science* **327,** 587–590 (2010).
5. DeWeese, M. R. & Zador, A. M. Non-Gaussian membrane potential dynamics imply sparse, synchronous activity in auditory cortex. *J. Neurosci.* **26,** 12206–12218 (2006).
6. Richardson, M. J. & Gerstner, W. Synaptic shot noise and conductance fluctuations affect the membrane voltage with equal significance. *Neural Comput.* **17,** 923–947 (2005).
7. Rudolph, M. & Destexhe, A. Characterization of subthreshold voltage fluctuations in neuronal membranes. *Neural Comput.* **15,** 2577–2618 (2003).
8. Tolhurst, D. J., Movshon, J. A. & Thompson, I. D. The dependence of response amplitude and variance of cat visual cortical neurones on stimulus contrast. *Exp. Brain Res.* **41,** 414–419 (1981).
9. Legenstein, R., Pecevski, D. & Maass, W. A learning theory for reward-modulated spike-timing-dependent plasticity with application to biofeedback. *PLOS Comput. Biol.* **4,** e1000180 (2008).
10. Thomson, A. M. & Lamy, C. Functional maps of neocortical local circuitry. *Front. Neurosci.* **1,** 19–42 (2007).
11. Steriade, M., Timofeev, I. & Grenier, F. Natural waking and sleep states: a view from inside neocortical neurons. *J. Neurophysiol.* **85,** 1969–1985 (2001).
12. Destexhe, A. & Pare, D. Impact of network activity on the integrative properties of neocortical pyramidal neurons *in vivo*. *J. Neurophysiol.* **81,** 1531–1547 (1999).
13. Crochet, S. & Petersen, C. C. Correlating whisker behavior with membrane potential in barrel cortex of awake mice. *Nature Neurosci.* **9,** 608–610 (2006).
14. Poulet, J. F. & Petersen, C. C. Internal brain state regulates membrane potential synchrony in barrel cortex of behaving mice. *Nature* **454,** 881–885 (2008).
15. Okun, M., Naim, A. & Lampl, I. The subthreshold relation between cortical local field potential and neuronal firing unveiled by intracellular recordings in awake rats. *J. Neurosci.* **30,** 4440–4448 (2010).
16. Hromadka, T., Zador, A. M. & Deweese, M. R. Up states are rare in awake auditory cortex. *J. Neurophysiol.* **109,** 1989–1995 (2013).
17. Peyrache, A. *et al.* Spatiotemporal dynamics of neocortical excitation and inhibition during human sleep. *Proc. Natl Acad. Sci. USA* **109,** 1731–1736 (2012).
18. Matsumura, M., Chen, D., Sawaguchi, T., Kubota, K. & Fetz, E. E. Synaptic interactions between primate precentral cortex neurons revealed by spike-triggered averaging of intracellular membrane potentials *in vivo*. *J. Neurosci.* **16,** 7757–7767 (1996).
19. Pei, X., Volgushev, M., Vidyasagar, T. R. & Creutzfeldt, O. D. Whole cell recording and conductance measurements in cat visual cortex *in vivo*. *Neuroreport* **2,** 485–488 (1991).
20. Ferster, D. & Jagadeesh, B. EPSP–IPSP interactions in cat visual cortex studied with *in vivo* whole-cell patch recording. *J. Neurosci.* **12,** 1262–1274 (1992).
21. Borg-Graham, L. J., Monier, C. & Fregnac, Y. Visual input evokes transient and strong shunting inhibition in visual cortical neurons. *Nature* **393,** 369–373 (1998).
22. Hirsch, J. A., Alonso, J. M., Reid, R. C. & Martinez, L. M. Synaptic integration in striate cortical simple cells. *J. Neurosci.* **18,** 9517–9528 (1998).
23. Kohn, A. & Smith, M. A. Stimulus dependence of neuronal correlation in primary visual cortex of the macaque. *J. Neurosci.* **25,** 3661–3673 (2005).
24. Nauhaus, I., Busse, L., Carandini, M. & Ringach, D. L. Stimulus contrast modulates functional connectivity in visual cortex. *Nature Neurosci.* **12,** 70–76 (2009).
25. Poulet, J. F., Fernandez, L. M., Crochet, S. & Petersen, C. C. Thalamic control of cortical states. *Nature Neurosci.* **15,** 370–372 (2012).
26. de Kock, C. P. & Sakmann, B. Spiking in primary somatosensory cortex during natural whisking in awake head-restrained rats is cell-type specific. *Proc. Natl Acad. Sci. USA* **106,** 16446–16450 (2009).
27. Brunel, N. Dynamics of sparsely connected networks of excitatory and inhibitory spiking neurons. *J. Comput. Neurosci.* **8,** 183–208 (2000).
28. Mehring, C., Hehl, U., Kubo, M., Diesmann, M. & Aertsen, A. Activity dynamics and propagation of synchronous spiking in locally connected random networks. *Biol. Cybern.* **88,** 395–408 (2003).
29. Cohen, M. R. & Maunsell, J. H. Attention improves performance primarily by reducing interneuronal correlations. *Nature Neurosci.* **12,** 1594–1600 (2009).
30. Mitchell, J. F., Sundberg, K. A. & Reynolds, J. H. Spatial attention decorrelates intrinsic activity fluctuations in macaque area V4. *Neuron* **63,** 879–888 (2009).

Supplementary Information is available in the online version of the paper.

Acknowledgements We thank T. Cakic for assistance with this project, and J. Hanover, D. Ferster, K. D. Miller and A. C. Huk for discussions and comments. A.Y.Y.T., B.S. and N.J.P. were supported by grants from the National Institutes of Health (NIH) (EY-019288) and the Pew Charitable Trusts; Y.C. and E.S. were supported by grants from the NIH (EY-016454 and EY-16752).

Author Contributions A.Y.Y.T., E.S. and N.J.P. initiated and designed the study. All authors collected the data, analysed the results, discussed the findings and wrote the paper. A.Y.Y.T., Y.C. and B.S. contributed equally to this work. E.S. and N.P. contributed equally to this work.

Author Information Reprints and permissions information is available at www.nature.com/reprints. The authors declare no competing financial interests. Readers are welcome to comment on the online version of the paper. Correspondence and requests for materials should be addressed to A.Y.Y.T. (atyy@alum.mit.edu) or N.J.P. (nico@austin.utexas.edu).

METHODS

All procedures were approved by the University of Texas Institutional Animal Care and Use Committee and conformed to National Institutes of Health standards. Our general experimental procedures in behaving macaque monkeys have previously been described in detail[31,32].

Behavioural task and visual stimulus. Three adult male macaque monkeys (*Macaca mulatta*) were trained to perform a visual fixation task in which gratings of different orientations were presented. Each trial began when a fixation spot was displayed at the centre of a monitor in front of the monkey. The monkey had to shift gaze to the fixation point and maintain fixation within a small window (less than 2° full width) for at least 1,500 ms to receive a reward. A drifting sinusoidal grating was presented at a randomized orientation for 1,000 ms while the monkey was maintaining strict fixation, thus minimizing variability due to eye movements. (See Supplementary Information and Extended Data Fig. 9 for characteristics of post-fixation saccades.)

Visual stimuli were presented on a gamma-corrected high-end 21-inch colour display (Sony Trinitron GDM-F520) at a fixed mean luminance of 30 cd m^{-2}. The display subtended 20.5° × 15.4° at a viewing distance of 108 cm and had a pixel resolution of 1,024 × 768, 30-bit colour depth and a refresh rate of 100 Hz. Visual stimuli were generated by using a high-end graphics card on a dedicated PC, using custom-designed software. Behavioural measurements and data acquisition were controlled by a PC running a software package for neurophysiological recordings from alert animals (Reflective Computing). Eye movements were measured with an infrared eye-tracking device (Dr Bouis).

Whole cell recordings. Recording chambers were located on the dorsal portion of V1, with the anterior portion of the chamber reaching close to the lunate sulcus and the border between V1 and V2. We verified the retinotopic organization by voltage-sensitive dye imaging[33], and by recording multiunit activity or local field potential with tungsten microelectrodes (Alpha Omega Co; MicroProbes for Life Sciences). The cortex in our cranial windows represents stimuli that are approximately 2.5°–5° away from the fovea in the lower quadrant of the contralateral hemifield.

Intracellular records of V_m (refs 18, 34, 35) were obtained with blind *in vivo* whole-cell recordings[19–22]. The recording chamber was filled with 2–4% agarose in artificial cerebrospinal fluid (CSF). Intracellular records were from neurons in the top 1,300 μm of V1. As a reference electrode, a silver–silver chloride wire was inserted into the agarose. The potential of the CSF was assumed to be uniform and equal to that of the reference electrode. Pipettes (6–12 MΩ) were pulled from borosilicate glass capillaries (KG-33, 1.2 mm outer diameter, 0.70 mm inner diameter; King Precision Glass) on a P-2000 micropipette puller (Sutter Instruments). Patch pipettes were filled with (in mM) 135 potassium gluconate, 4 NaCl, 0.5 EGTA, 2 $MgATP^{2-}$, 10 phosphocreatine disodium, 10 HEPES, pH adjusted to 7.3 with KOH (Sigma–Aldrich). Whole-cell current-clamp recordings were performed with an Axoclamp 2B Microelectrode Amplifier (Molecular Devices). We subtracted 7 mV from all raw membrane potential values to compensate for the liquid junction potential[36]. (See Supplementary Information and Extended Data Fig. 10 for intrinsic properties of recorded neurons.)

Data analysis. We analysed V_m during the fixation period in trials during which the monkey performed the task successfully, provided that the mean V_m in the absence of a visual stimulus was less than −50 mV. V_m was detrended by high-pass filtering at 0.1 Hz. Data were analysed with MATLAB (Mathworks). Shot noise contributions to V_m were assessed by the skewness[6,37–39] of V_m distributions. Coherence estimates were performed with Chronux[40], a MATLAB library (freely available from http://chronux.org/).

Data analysis for Supplementary Information. The relationship between spike rate R and V_m was described with a threshold followed by a power law[41–43]: $R = A[V_m - V_{th}]_+^p$, where A is a fitted constant, V_{th} is the resting membrane potential, + indicates rectification, and p is the fitted exponent. Orientation selectivity was assessed with an orientation selectivity index[44,45] (vector average = 1 − circular variance). Temporal modulation was assessed with the Fourier component of the response with the same temporal frequency as the moving sinusoidal grating visual stimulus divided by the time-averaged response[46] (F_1/F_0). Simulations of Hodgkin–Huxley neurons used parameters adapted from refs 47 and 48, and were performed with Brian[49,50]. We estimated membrane conductance from voltage responses to hyperpolarizing current pulses of constant amplitude, and a fit of a sum of two exponentials to the voltage response[51]:

$$V(t) = I_{inj}[(R_M(1-\exp(-t/\tau_M))) + (R_E(1-\exp(-t/\tau_E)))]$$

where V is the voltage response, t is time, I_{inj} is injected current, R_M is membrane resistance, τ_M is membrane time constant, R_E is electrode resistance and τ_E is electrode time constant. Membrane conductance is $1/R_M$.

31. Chen, Y., Geisler, W. S. & Seidemann, E. Optimal decoding of correlated neural population responses in the primate visual cortex. *Nature Neurosci.* **9,** 1412–1420 (2006).
32. Chen, Y., Geisler, W. S. & Seidemann, E. Optimal temporal decoding of neural population responses in a reaction-time visual detection task. *J. Neurophysiol.* **99,** 1366–1379 (2008).
33. Yang, Z., Heeger, D. J. & Seidemann, E. Rapid and precise retinotopic mapping of the visual cortex obtained by voltage-sensitive dye imaging in the behaving monkey. *J. Neurophysiol.* **98,** 1002–1014 (2007).
34. Matsumura, M. Intracellular synaptic potentials of primate motor cortex neurons during voluntary movement. *Brain Res.* **163,** 33–48 (1979).
35. Chen, D. & Fetz, E. E. Characteristic membrane potential trajectories in primate sensorimotor cortex neurons recorded *in vivo*. *J. Neurophysiol.* **94,** 2713–2725 (2005).
36. Margrie, T. W., Brecht, M. & Sakmann, B. *In vivo*, low-resistance, whole-cell recordings from neurons in the anaesthetized and awake mammalian brain. *Pflugers Arch.* **444,** 491–498 (2002).
37. Richardson, M. J. & Gerstner, W. Statistics of subthreshold neuronal voltage fluctuations due to conductance-based synaptic shot noise. *Chaos* **16,** 026106 (2006).
38. Richardson, M. J. & Swarbrick, R. Firing-rate response of a neuron receiving excitatory and inhibitory synaptic shot noise. *Phys. Rev. Lett.* **105,** 178102 (2010).
39. Wolff, L. & Lindner, B. Method to calculate the moments of the membrane voltage in a model neuron driven by multiplicative filtered shot noise. *Phys. Rev. E* **77,** 041913 (2008).
40. Mitra, P. & Bokil, H. *Observed Brain Dynamics* (Oxford Univ. Press, 2008).
41. Miller, K. D. & Troyer, T. W. Neural noise can explain expansive, power-law nonlinearities in neural response functions. *J. Neurophysiol.* **87,** 653–659 (2002).
42. Hansel, D. & van Vreeswijk, C. How noise contributes to contrast invariance of orientation tuning in cat visual cortex. *J. Neurosci.* **22,** 5118–5128 (2002).
43. Priebe, N. J., Mechler, F., Carandini, M. & Ferster, D. The contribution of spike threshold to the dichotomy of cortical simple and complex cells. *Nature Neurosci.* **7,** 1113–1122 (2004).
44. Swindale, N. V. Orientation tuning curves: empirical description and estimation of parameters. *Biol. Cybern.* **78,** 45–56 (1998).
45. Ringach, D. L., Shapley, R. M. & Hawken, M. J. Orientation selectivity in macaque V1: diversity and laminar dependence. *J. Neurosci.* **22,** 5639–5651 (2002).
46. Skottun, B. C. *et al.* Classifying simple and complex cells on the basis of response modulation. *Vision Res.* **31,** 1079–1086 (1991).
47. Destexhe, A., Rudolph, M., Fellous, J. M. & Sejnowski, T. J. Fluctuating synaptic conductances recreate *in vivo*-like activity in neocortical neurons. *Neuroscience* **107,** 13–24 (2001).
48. Pospischil, M. *et al.* Minimal Hodgkin–Huxley type models for different classes of cortical and thalamic neurons. *Biol. Cybern.* **99,** 427–441 (2008).
49. Goodman, D. & Brette, R. Brian: a simulator for spiking neural networks in python. *Front. Neuroinform.* **2,** 5 (2008).
50. Goodman, D. F. & Brette, R. The Brian simulator. *Front. Neurosci.* **3,** 192–197 (2009).
51. Anderson, J. S., Carandini, M. & Ferster, D. Orientation tuning of input conductance, excitation, and inhibition in cat primary visual cortex. *J. Neurophysiol.* **84,** 909–926 (2000).

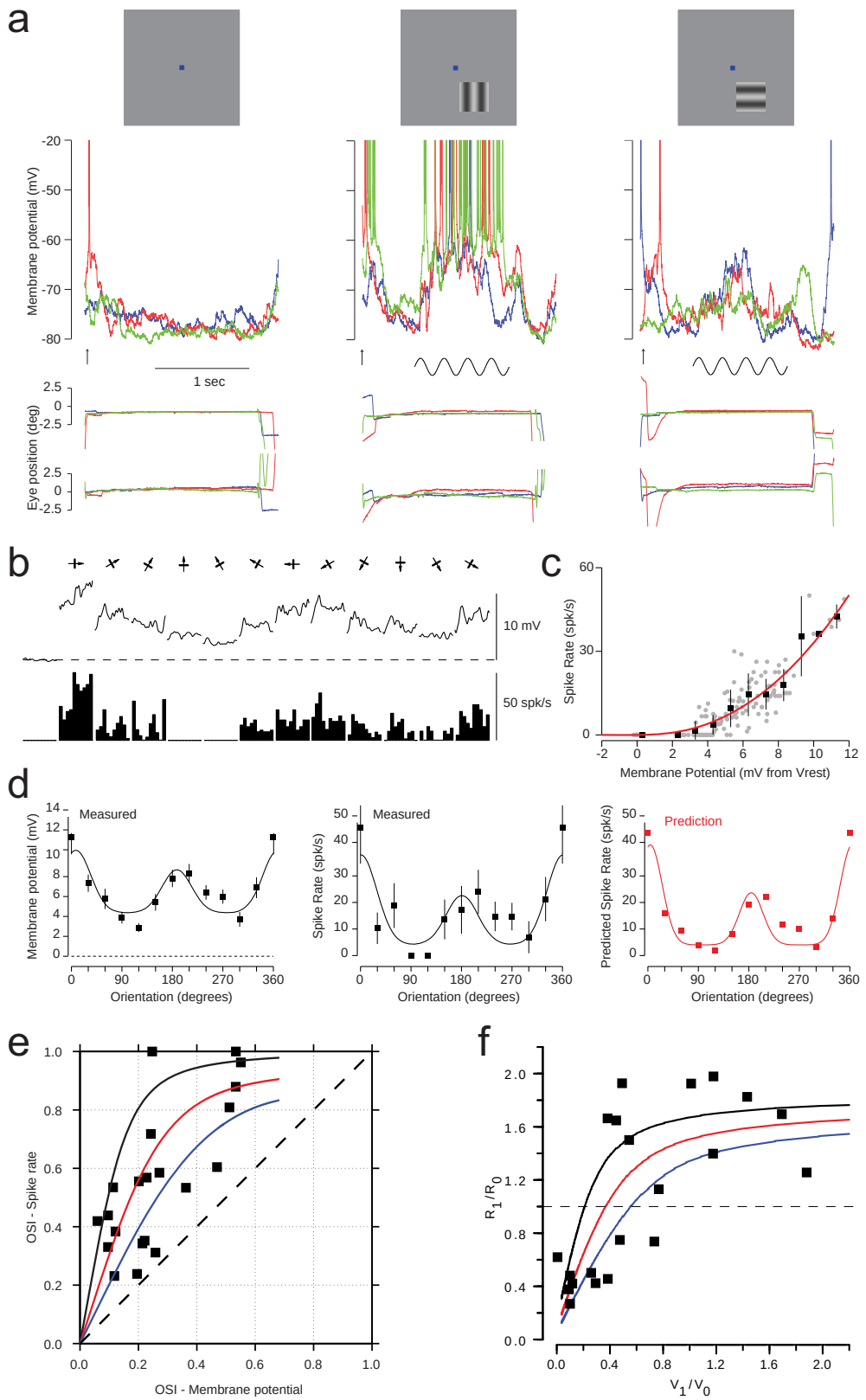

Extended Data Figure 1 | Orientation tuning of V_m and spike rate. **a**, V_m responses (top traces), eye position traces (bottom pairs of traces) from three blank trials (left), three trials at the preferred orientation (centre), and three trials at the orthogonal orientation (right). **b**, Trial averaged V_m (top) and spike rate (bottom) for all orientations, from the neuron in **a**. **c**, Spike rate versus membrane potential, and best-fit thresholded power law, from the neuron in **a**. **d**, Orientation tuning curves for V_m and spike rate, and predicted spike rate orientation tuning curve using the V_m orientation tuning curve and the best-fit thresholded power law in **c**, from the neuron in **a**. **e**, Orientation selectivity index (OSI) for spike rate versus OSI for V_m. Lines represent expected relationships between spike rate OSI and V_m OSI for thresholded power laws with exponents 2, 3 and 5 (blue, red and black, respectively). **f**, Fourier component of the response with the same temporal frequency as the moving sinusoidal grating visual stimulus divided by the time-averaged response for spike rate (R_1/R_0) versus that for V_m (V_1/V_0). Lines represent expected relationships between R_1/R_0 and V_1/V_0 for thresholded power laws with exponents 2, 3 and 5 (blue, red and black, respectively).

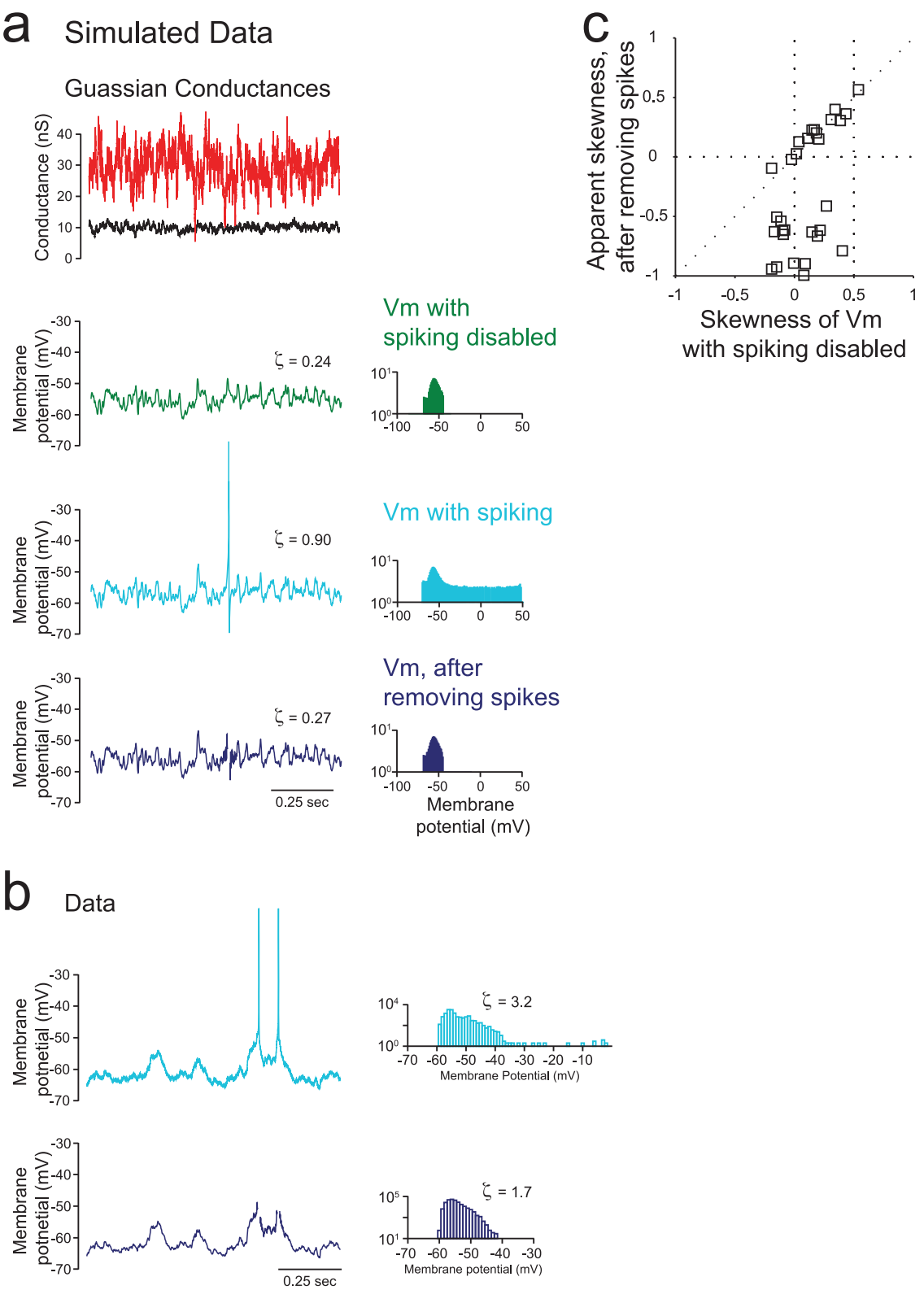

Extended Data Figure 2 | Estimation and implication of V_m skewness during blank trials. **a**, Gaussian excitatory (black) and inhibitory (red) conductances, V_m with spiking disabled (green), V_m with spiking enabled (light blue), and V_m with spikes removed (dark blue), and corresponding V_m amplitude histograms and skewness values ζ, for a simulated neuron with Hodgkin–Huxley conductances. **b**, V_m with spiking (light blue) and with spikes removed (dark blue) and corresponding V_m amplitude histograms and skewness values ζ, for a recorded neuron. **c**, Apparent skewness from V_m with spikes removed versus skewness from V_m with spiking disabled from a simulated neuron with Hodgkin–Huxley conductances, for a range of Gaussian inputs.

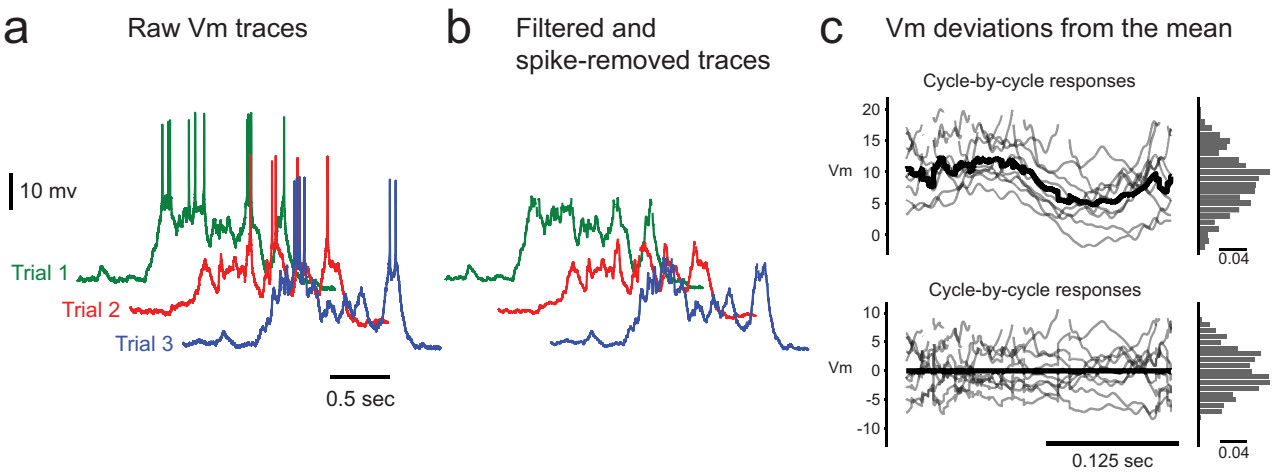

Extended Data Figure 3 | Estimation of V_m skewness during visual stimulation trials. **a**, Raw traces from several trials. **b**, Traces after bandpass filtering and spike removal. **c**, V_m responses from each cycle (top grey traces), cycle-averaged response (top black trace) and histogram of V_m responses (top histogram); residual traces from each cycle after subtraction of cycle-averaged response (bottom grey traces), cycle-averaged residuals (bottom black trace) and histogram of V_m residuals (bottom histogram). Note the change in vertical scale from top to bottom panels.

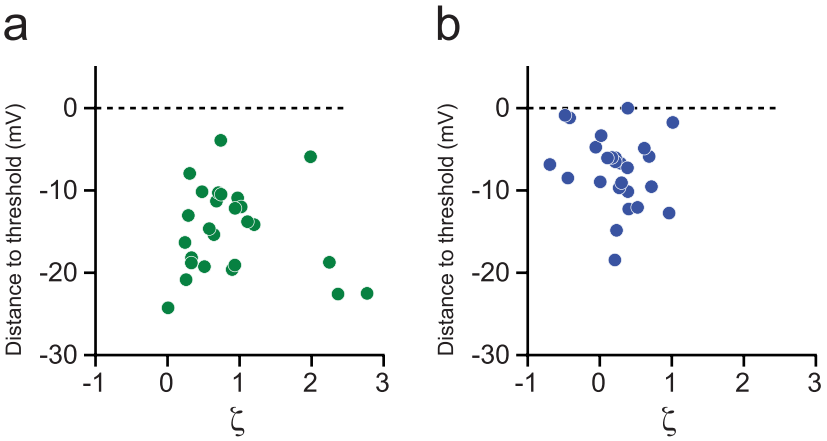

Extended Data Figure 4 | Joint distribution of V_m–threshold distance and skewness. **a**, Joint distribution of V_m–threshold distance and skewness ζ during blank trials. **b**, Joint distribution of V_m–threshold distance and skewness ζ during preferred orientation trials.

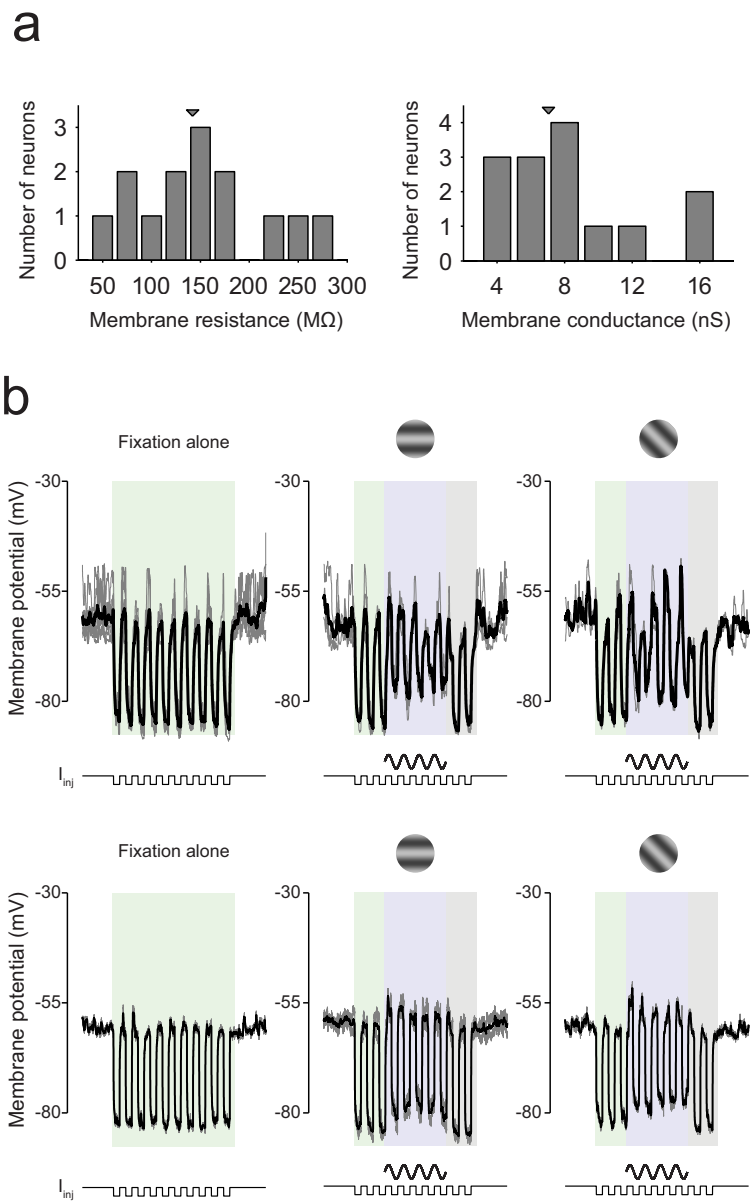

Extended Data Figure 5 | Membrane conductance during blank and visual stimulation trials. **a**, Distribution of membrane resistance (left) and corresponding membrane conductance (right) during blank trials. **b**, Change in membrane conductance during visual stimulation in two example neurons during blank (left), preferred (centre) and 45° from preferred (right) trials. Each row shows data from a different neuron.

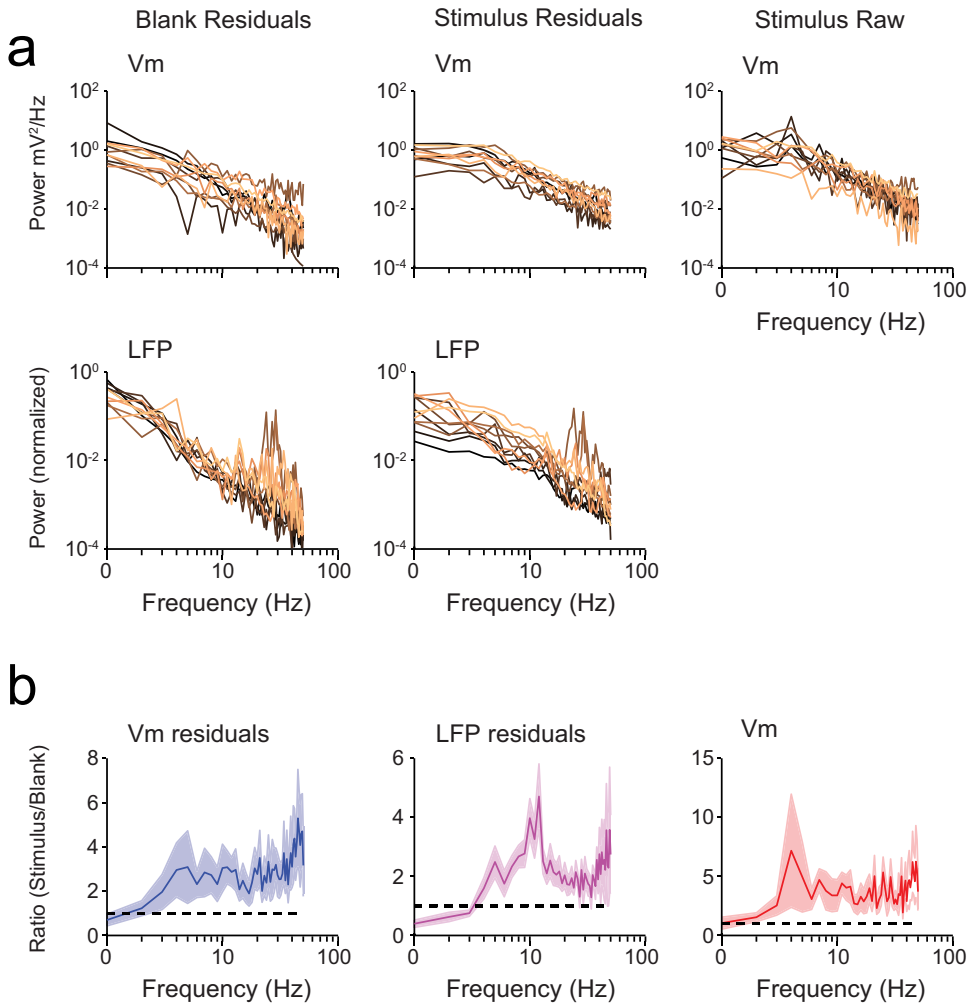

Extended Data Figure 6 | Power spectra of V_m and LFP fluctuations from the trial average. **a**, Power spectrum of V_m (top panels) and LFP (bottom panels) fluctuations from the trial average (residuals) during blank trials (left panels), residuals during preferred orientation stimulation (middle panels), and raw V_m traces during preferred orientation stimulation (right panel). Each trace corresponds to an individual neuron. **b**, Population-averaged ratio of power spectrum at the preferred orientation to power spectrum for blank trials for V_m fluctuations from the trial average ('V_m residuals', left panel), LFP fluctuations from the trial average ('LFP residuals', middle panel), and raw V_m (right panel). Error bars are jack-knifed standard errors.

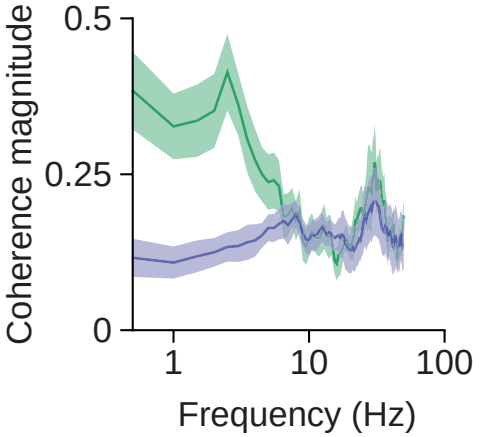

Extended Data Figure 7 | V_m–LFP coherence magnitude for blank trials and visual stimulation. Population-averaged V_m–LFP coherence magnitudes for blank trials (green) and at the preferred orientation (lavender). Error bars are jack-knifed standard errors.

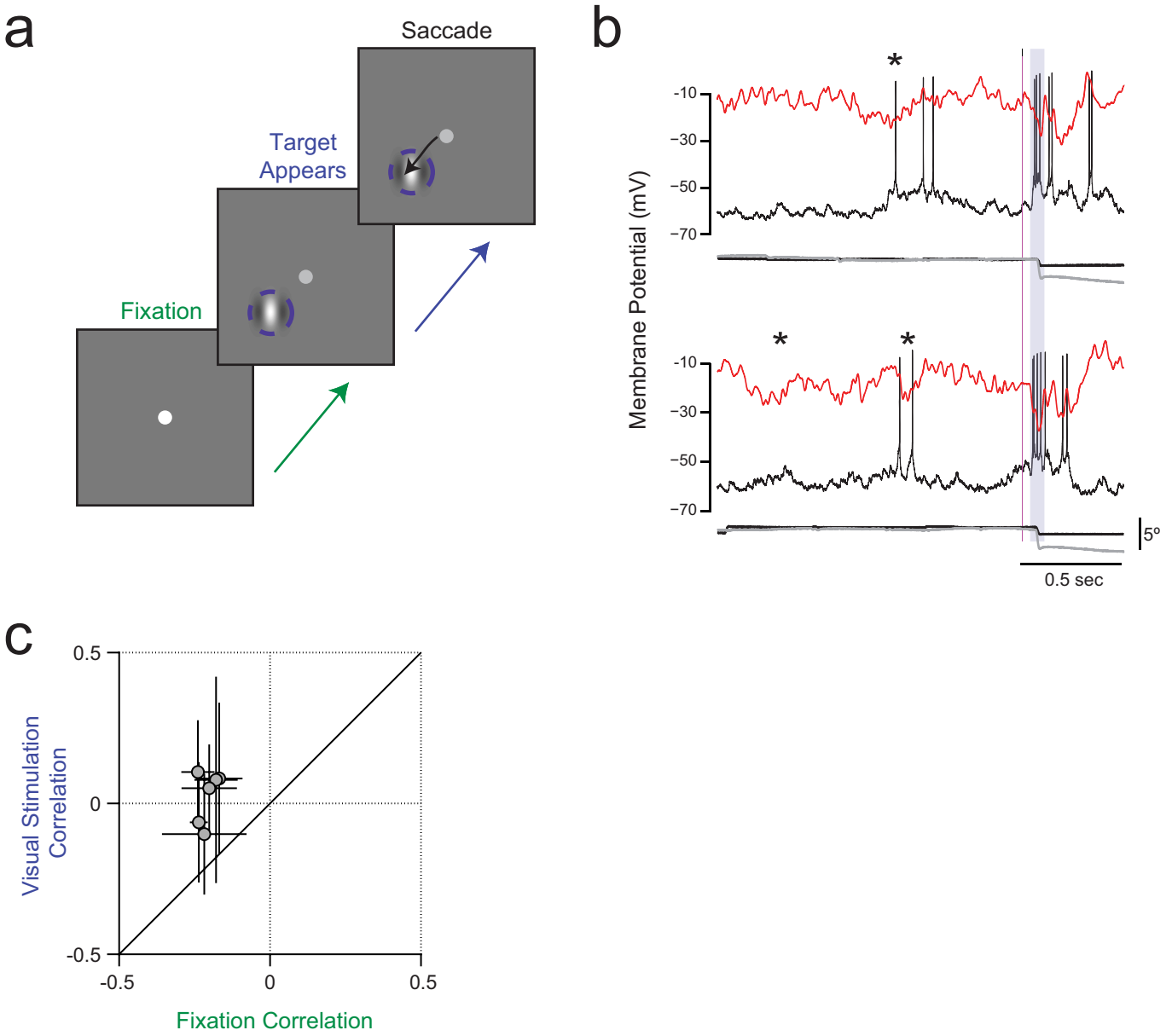

Extended Data Figure 8 | Decreased magnitude of V_m–LFP correlation during a flashed stimulus in a visual saccade task. **a**, Each trial began when a fixation spot was displayed at the centre of a monitor in front of the monkey. The monkey had to shift gaze to the fixation point and maintain tight fixation for at least 1,500 ms. A flashed Gabor target stimulus appeared at a random time between 1,000 and 1,500 ms after the monkey had established tight fixation. The monkey had to saccade to the target stimulus within 600 ms to receive a reward. We analysed V_m and LFP only from trials in which the monkey performed the task successfully. **b**, Simultaneously recorded V_m and LFP, as well as eye movement traces, in two trials from an example neuron. Asterisks indicate near-simultaneous deflections in V_m and LFP during the pre-stimulus fixation period. Grey shading indicates the analysis period for correlations during the flashed Gabor stimulus; we included 30 ms after saccade onset in this period, because the visual latency for spike responses in the lateral geniculate nucleus is greater than 30 ms. **c**, Zero-lag cross-correlation between V_m and LFP fluctuations from the trial average during the flashed Gabor stimulus versus during the pre-stimulus period.

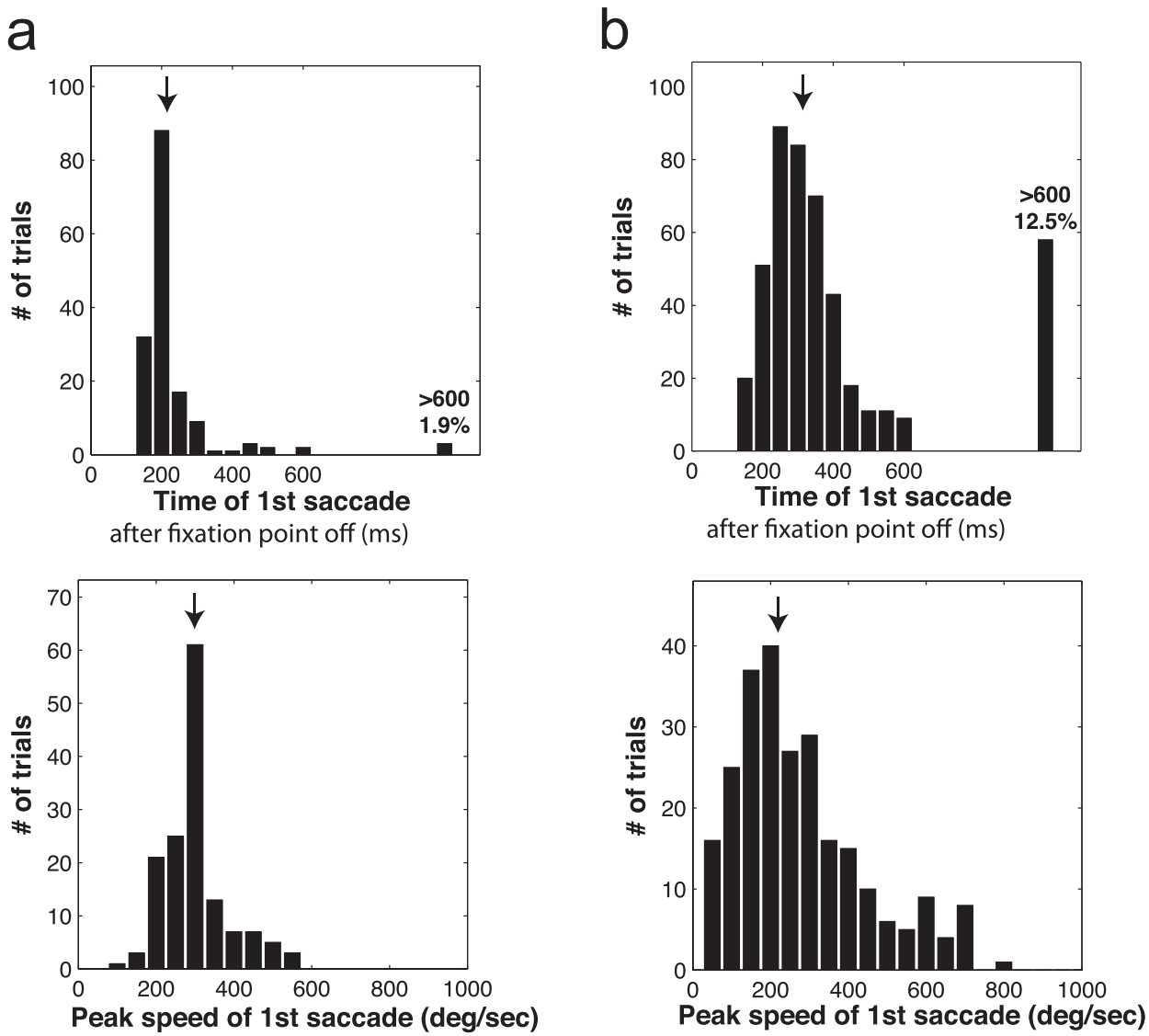

Extended Data Figure 9 | Summary of first saccade latency and peak velocity in monkeys T and W, which together contributed the majority of the recorded data. **a**, Top: histogram of latency of first saccade after fixation point termination in three neurons (158 trials) in monkey W. Arrow indicates median latency (217 ms). In 1.9% of the trials no saccade was detected in the 600 ms after fixation point termination. Bottom: histogram of peak eye velocity for first saccades during the 600 ms after fixation point offset. Arrow indicates median peak velocity (292° s^{-1}). **b**, Results from eight neurons (464 trials) in monkey T. The format is the same as in **a**. Median latency is 314 ms and median peak velocity is 229° s^{-1}. Monkey W tended to make larger saccades away from fixation, whereas monkey T tended to make smaller saccades and in a small subset of the trials remained close to the fixation point location until the next trial was initiated. This may reflect the fact that the minimal inter-trial interval was shorter in monkey T than in monkey W. The short latency of the saccades after fixation point termination in the vast majority of the trials indicates that both monkeys were alert and attentive and were actively engaged in maintaining tight fixation.

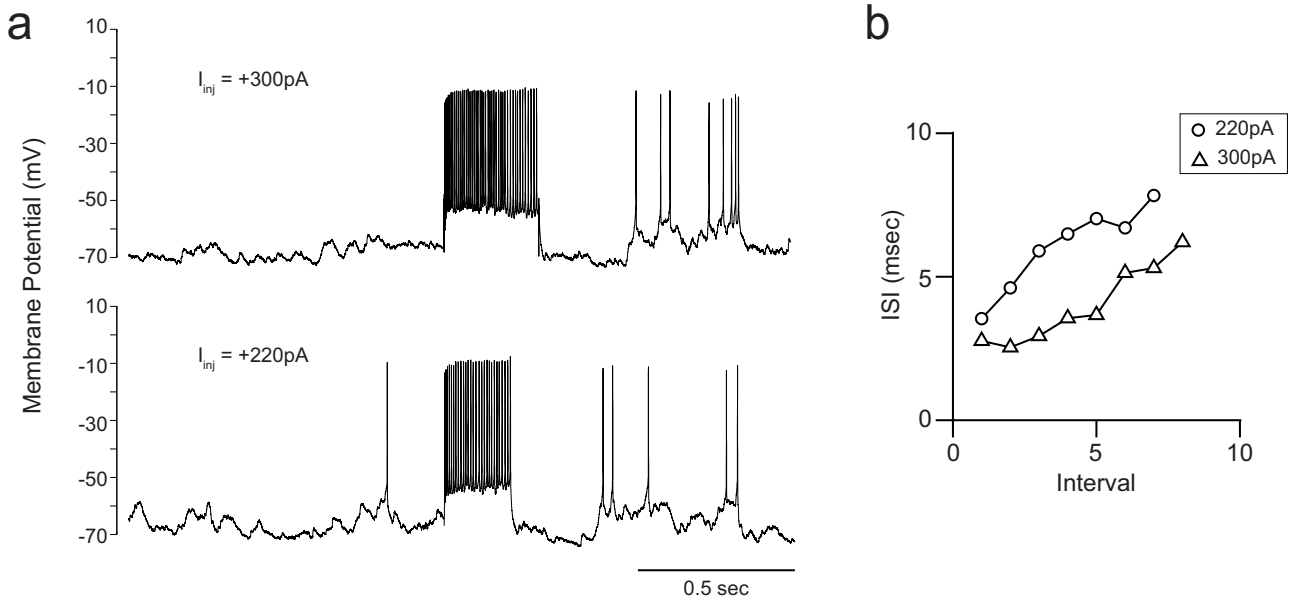

Extended Data Figure 10 | Regular-spiking neurons. **a**, V_m response to injections of current steps of different magnitudes in an example neuron. **b**, Interspike interval during the current step versus interval ordinal. The interspike interval increased with interval ordinal, indicating that this neuron was regular-spiking.